Chemical Science

ROYAL SOCIETY OF CHEMISTRY

EDGE ARTICLE

View Article Online
View Journal | View Issue

Cite this: *Chem. Sci.*, 2023, **14**, 10500

All publication charges for this article have been paid for by the Royal Society of Chemistry

Received 21st April 2023
Accepted 20th August 2023

DOI: 10.1039/d3sc02077k

rsc.li/chemical-science

Insights into the synthesis of NHC-stabilized Au nanoclusters through real-time reaction monitoring†

Junliang Liu,‡[a] Yusuke Sato,‡[a] Viveka K. Kulkarni,[bc] Angus I. Sullivan,[bc] Wenyu Zhang,[a] Cathleen M. Crudden *[bcd] and Jason E. Hein *[aef]

Atomically precise gold nanoclusters (AuNCs) are interesting nanomaterials with potential applications in catalysis, bioimaging and optoelectronics. Their compositions and properties are commonly evaluated by various analytical techniques, including UV-vis spectroscopy, NMR spectroscopy, ESI mass spectrometry, and single-crystal X-ray diffraction. While these techniques have provided detailed insights into the structure and properties of nanoclusters, synthetic methods still suffer from a lack of *in situ* and real-time reaction monitoring methodologies. This limits insight into the mechanism of formation of AuNCs and hinders attempts at optimization. We have demonstrated the utility of HPLC-MS as a monitoring methodology in the synthesis of two NHC-protected gold nanoclusters: $[Au_{13}(NHC)_9Cl_3]^{2+}$ and $[Au_{24}(NHC)_{14}Cl_2H_3]^{3+}$. Herein we show that HPLC coupled with mass spectrometry and ^{13}C NMR spectroscopy of labelled derivatives enables new insight into critical reaction dynamics of AuNCs synthesis and rapid reaction optimization.

Introduction

Atomically precise gold nanoclusters (AuNCs) are a unique type of nanomaterial[1,2] that can be isolated as monodisperse species with defined molecular formulae.[3,4] They possess molecule-like properties such as discrete absorption bands, and can be characterized by molecular techniques.[2,5] Among reported AuNCs, those protected by N-heterocyclic carbenes (NHCs) have gained increasing attention due to their remarkable quantum yields, high stability, and catalytic activity.[6–10] Analytical techniques including excitation–emission fluorescence spectroscopy,[11] ultraviolet-visible (UV-vis) spectroscopy,[12] single crystal X-ray diffraction (SCXRD)[13,14] and nuclear magnetic resonance (NMR) spectroscopy[15] have been employed to provide detailed descriptions of the structure of NHC-stabilized AuNCs.

In the wider realm of thiolate-stabilized AuNCs, the use of process analytical technology (PAT) to monitor synthetic reactions in real time has been employed but remains challenging due to the lack of a single, observable starting material, the complexity of AuNC reaction mixtures and the evolving nature of the AuNCs.[4,16,17] When synthesizing thiolate-stabilized AuNCs, UV-vis[18] and mass spectrometry[19,20] are typically employed. These methods can provide ensemble measurements of the mixture of materials in the reaction media but require spectral deconvolution to identify individual species that may be present. This can limit the granularity with which the cluster formation mechanisms can be studied and hinders the ability to optimize synthetic conditions.[21]

Reverse phase HPLC (RP-HPLC) has been used to effectively separate AuNC mixtures stabilized by various ligands[22,23] and to provide information about product and side-product compositions with high deconvolution capabilities.[24,25] Despite this, HPLC methods are still limited to end-point analysis or preparative purposes in the field of NCs synthesis, even though the ability to monitor a process as it occurs yields far more information.[26–28]

We report herein the use of continuous reaction monitoring in the synthesis of NHC-protected AuNCs by HPLC-MS and the introduction of a regional analysis methodology for nanocluster synthesis. We chose to study the preparation of two nanoclusters previously (Fig. 1) reported by Crudden *et al.* because of the importance of the Au_{13} core structure, the stability of the clusters and the potential to see interconversion between different species.[29,30] The effect of temperature, HCl etching and reductant dosing rate are all explored using LC-MS and analysed using a regional analysis methodology by defining small,

[a]*Department of Chemistry, The University of British Columbia, Vancouver, BC V6T 1Z1, Canada. E-mail: jhein@chem.ubc.ca*

[b]*Department of Chemistry, Queen's University, Kingston, ON, K7L 3N6, Canada. E-mail: cruddenc@chem.queensu.ca*

[c]*Carbon to Metal Coatings Institute, Queen's University, Kingston, ON, Canada*

[d]*Institute of Transformative Bio-Molecules (WPI-ITbM), Nagoya University, Nagoya 464-8602, Japan*

[e]*Acceleration Consortium, University of Toronto, ON, Canada*

[f]*Department of Chemistry, University of Bergen, N-5007, Bergen, Norway*

† Electronic supplementary information (ESI) available: Synthesis, HPLC traces and methodologies and NMR data. See DOI: https://doi.org/10.1039/d3sc02077k

‡ These authors contributed equally.

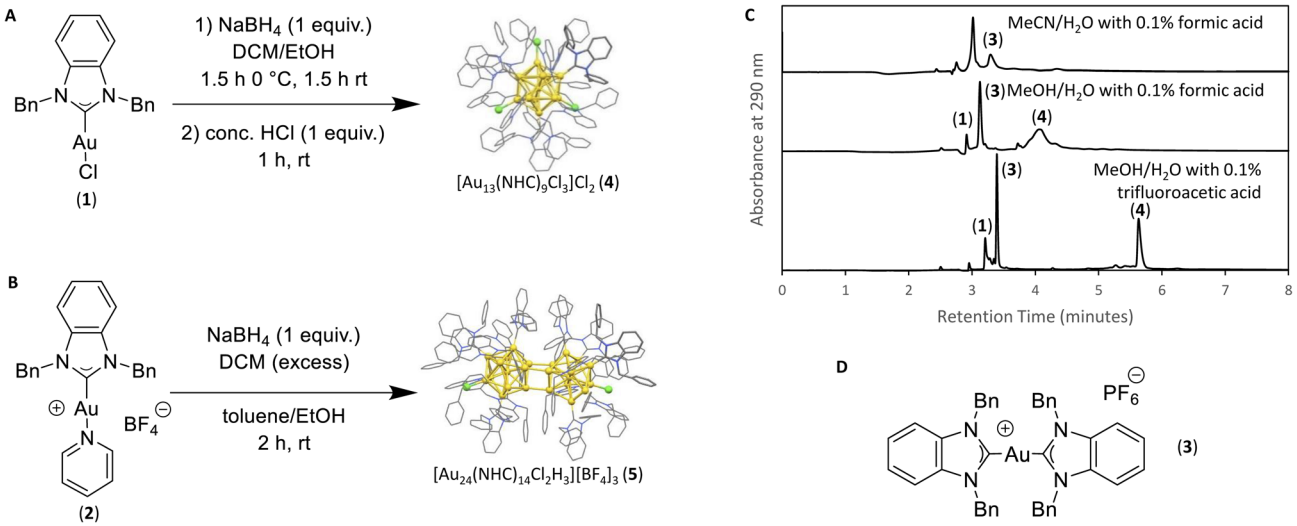

Fig. 1 (A) Conditions for the synthesis of **4** (B) conditions used for the synthesis of **5**, (C) chromatogram for the optimization of HPLC methods showing the effective separation of major species in synthesis of **4**. (D) Structure of byproduct (**3**).

medium and large *m*/*z* regions of HPLC chromatograms. The use of NHC ligands isotopically enriched at the carbene carbon enabled added insight through ^{13}C NMR spectroscopy. These techniques allowed us to identify previously unknown intermediates and provided valuable mechanistic insights.

Results and discussion

Nanocluster synthesis

Following previous reports from Crudden *et al.*, starting materials **1** and **2** were prepared for use in the synthesis of the desired clusters.[7,30] Known by-product $[NHC–Au(I)–NHC]^+$ (**3**), was synthesized *via* an adapted literature procedure, namely reaction between the $[NHC][PF_6]$ salt, 1 equiv. of base, and starting material (**1**).[7,30,31] Cluster **4** ($[Au_{13}(NHC)_9Cl_3]Cl_2$) was synthesized by dissolving NHC–Au–Cl (**1**) in DCM followed by the addition of 1 equiv. $NaBH_4$ dissolved in EtOH. The reaction mixture was stirred at 0 °C for 1 hour, followed by two hours at room temperature. After this time, 1 equiv. HCl was added, and the resulting mixture was purified by column chromatography (1 : 10 MeOH/DCM). To prepare cluster **5**, ($[Au_{24}(NHC)_{14}Cl_2H_3][BF_4]_3$), $[NHC–Au–Py]BF_4$ (**2**) was dissolved in toluene and 1 equiv. $NaBH_4$ dissolved in EtOH was added. The reaction was stirred at 0 °C and allowed to warm to room temperature over 7 hours. The resulting mixture was purified by column chromatography (1 : 12 MeOH/DCM). These methods were adapted for the preparation of HPLC scale reactions (see ESI Section 3.2†).

HPLC and analytical method development§

Initial efforts to develop an HPLC method to monitor cluster formation focused on $[Au_{13}(NHC)_9Cl_3]Cl_2$ (**4**) as the major product[7] and **1** and **3** (Fig. 1D) as known by-products in the cluster synthesis. Three different HPLC mobile phases were tested to separate these three components using a solvent gradient in which the percentage of water was changed from 5% to 100% over 2.3 minutes (Fig. 1C). The addition of 0.1% trifluoroacetic acid (TFA) to the H_2O/MeOH resulted in good resolution of **1**, **3**, and **4** with sufficiently short elution time enabling frequent sampling over the length of AuNC synthesis (Fig. 1C).

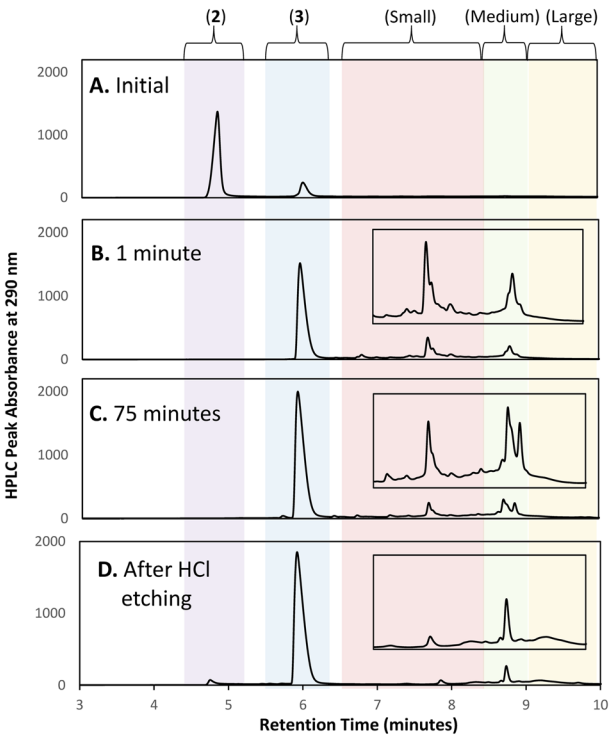

Fig. 2 Chromatograms of the synthesis of **4** taken at four critical points in the reaction with regional analysis zones identified and highlighted. Sample taken before the addition of $NaBH_4$ (A), immediately following addition of $NaBH_4$ (B), after 75 minutes of reaction time (C), and after HCl etching (D).

We then moved to the analysis of actual reaction mixtures, taking samples at various stages of cluster formation[7] (Fig. 2). After the addition of $NaBH_4$, several new species were observed indicating the formation of various AuNCs and larger amounts of **3** (Fig. 2B and C). The addition of concentrated HCl decreased the intensity of most of the peaks with the exception of cluster **4** (Fig. 2D), supporting the occurrence of a "size-focusing" process as proposed in the literature, and the inherent stability of the Au_{13} cluster.¶[10,29]

Regional analysis method development

To simplify the analysis, we employed a regional methodology, splitting the chromatogram into five size regions. This approach was based on reports that RP-HPLC can separate AuNCs by molecular weight:[22,23] species with a lower mass-to-charge ratio (*m*/*z*) have shorter retention times, and those with larger *m*/*z* ratios have longer retention times. These suppositions were confirmed by mass spectrometry of the species present in the three nanocluster areas (ESI, Fig. S3–S36†). HRMS was used to confirm the isotope pattern of the identified clusters and compare with the theoretical pattern of the species supporting the presence of a previously unidentified, Au_{14}-based nanocluster (ESI, Section S8.4†).

The small *m*/*z* region of the chromatogram was defined to include species with retention times of 6.5 to 8.5 minutes (*m*/*z* 1000–2600), the medium *m*/*z* region, contains (**4**) and other by-products and extends from 8.5 to 9 minutes (*m*/*z* 2600–3000), and the large *m*/*z* region contains all species with retention times > 9 minutes (*m*/*z* > 3000) (Fig. 2).‖

Reaction monitoring during synthesis of $[Au_{13}(NHC)_9Cl_3]Cl_2$ (4)

With the analytical method in hand, the synthesis of **4** was affected following the literature procedure (Fig. 1A) with continual sampling and MS analysis.[7] The addition of $NaBH_4$ results in complete consumption of **1** by the time the first data point is acquired after $NaBH_4$ addition (1 min). At this point, the amount of **3** has increased dramatically, and clusters are already obvious in the small and medium *m*/*z* region (Fig. 3). The appearance of **3** concurrent with the formation of clusters suggests that it is a sink for NHCs released during cluster formation. Structurally related complexes are also observed as by-products in thiolate-protected AuNC synthesis.[20]

Over the next 1.5 hours, the growth rate of the medium *m*/*z* region slowed, and the total peak area representing species in the small *m*/*z* region gradually diminished. This was coupled with the slow growth of AuNCs in the large *m*/*z* region. These results provide evidence that the formation of large AuNCs occurs through smaller intermediates.

After 1.5 hours at 0 °C, the reaction was warmed to room temperature, at which point transformations between clusters in different size regimes appeared to accelerate. In the first 30 minutes after warming, the peak area of clusters in the small *m*/*z* region decreased rapidly, while the medium *m*/*z* region remained unchanged. Signals attributed to the large *m*/*z* region grew, and some amount of **1** was reformed. After the full consumption of the small-sized species, clusters in the large *m*/*z* region began forming more rapidly. Interestingly, the consumption of medium-sized clusters only occurs at this point. These results support the possibility that clusters grow sequentially from the small to medium to large species. The re-emergence of **1** is attributed to the decomposition of more thermally unstable intermediates as the temperature is increased.

These observations were confirmed by $^{13}C\{^1H\}$ NMR spectroscopy employing a ^{13}C labelled isotopologue of **3** (ESI, Fig. S52 and S53†). Conditions used in the LC-MS experiments were replicated in an NMR tube and $^{13}C\{^1H\}$ NMR confirmed immediate consumption of ^{13}C-**1**, slow formation of ^{13}C-**3**, and reformation of ^{13}C-**1** after the reaction mixture was warmed to room temperature.

Clusters that appeared in the medium *m*/*z* region appear to be the critical zone under examination, chiefly because the targeted Au_{13} cluster (**4**) resides within this section, along with **5**, and a novel cluster characterized by an *m*/*z* of 2774 (Fig. 4E). HRMS analysis suggests that this gold nanocluster has the formula $[Au_{14}(NHC)_9Cl_3]^{2+}$.

A more detailed analysis of signals in this region is complicated by the presence of overlapping peaks. Since changes to the chromatographic conditions, including a wide survey of new solid and liquid phases, did not yield improved separation, we formulated a peak-deconvolution algorithm specifically designed to prevent overfitting[32] (ESI, Section S2.4†) (Fig. 4). This enables us to create a semiquantitative interpretation of the change in species by integrating each peak more accurately within this region as shown in Fig. 5.

Using this analysis, the predominant peak in the medium region after $NaBH_4$ addition is the Au_{14} cluster (Fig. 5). After 30 minutes at 0 °C, signals attributed to species **4** and **5** increase, while that of Au_{14} decrease. As the reaction progresses at 0 °C, a continuous decline in Au_{14} is observed, coupled with a rise in

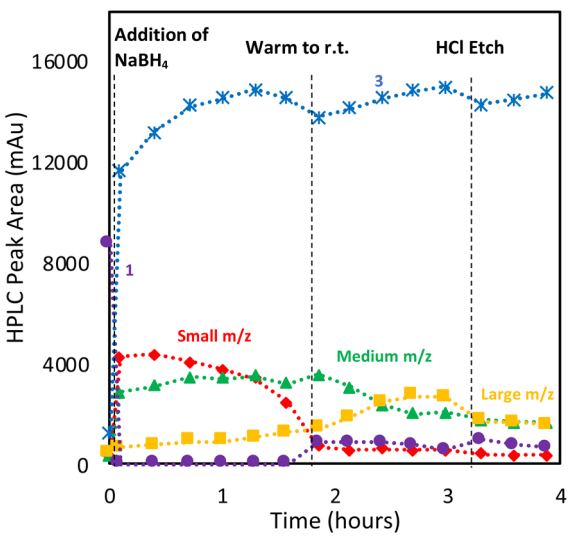

Fig. 3 HPLC monitoring of major products and regional analysis size regions in the synthesis of (**4**). Blue star (**3**), red diamond (small region), green triangle (medium region), yellow square (large region), purple circle (**1**). The first data point after the zero point was obtained 1 minute after addition of $NaBH_4$.

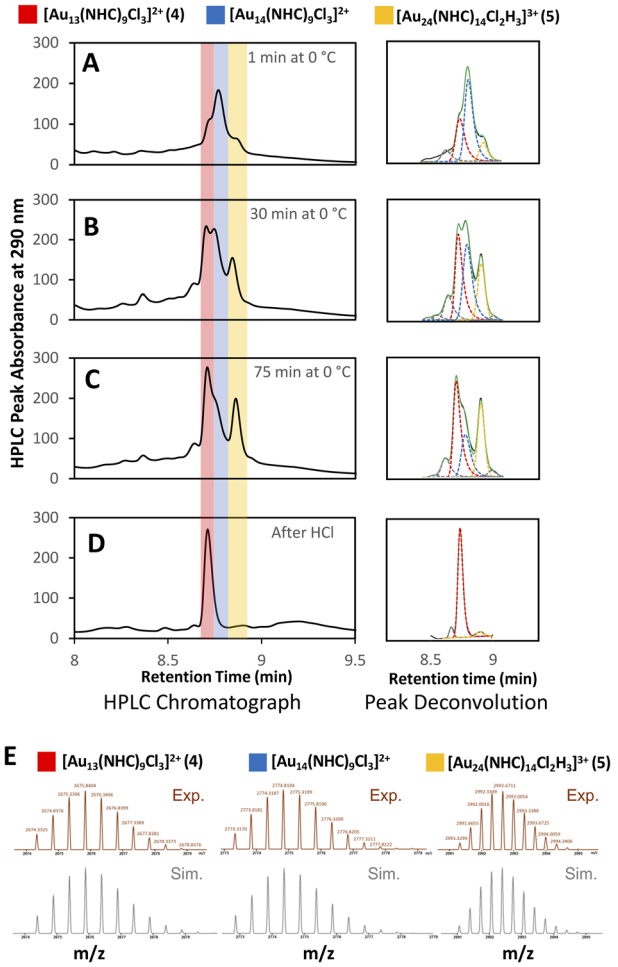

Fig. 4 The medium region of the HPLC chromatogram, deconvoluted peaks to quantify the major identified Au nanoclusters, and the HRMS of the red, blue and yellow regions. Reaction chromatograms are displayed from time points immediately after $NaBH_4$ addition (A), at 30 min following $NaBH_4$ addition (B), after 75 minutes (C), and after HCl etch (D). (E) Experimental HRMS of nanoclusters observed during this reaction sequence; $[Au_{13}(NHC)_9Cl_3]^{2+}$ (**4**), $[Au_{24}(NHC)_{14}Cl_2H_3]^{3+}$ (**5**) and the novel $[Au_{14}(NHC)_9Cl_3]^{2+}$.

4 and **5**. When the reaction is warmed to room temperature, all three peaks decline in peak area, consistent with the appearance of clusters in the "large" region (Fig. 3).

Following the introduction of concentrated HCl, both Au_{14} and **5** decrease almost completely while the amount of cluster **4** present remains constant. This analysis confirms the role of HCl as an etchant that degrades less stable gold nanoclusters, leaving the more stable Au_{13} as the predominant product.

Examination of the reaction performed with ^{13}C-labeled **1** by $^{13}C\{^1H\}$ NMR spectroscopy 1 minute after the addition of $NaBH_4$ supported the suggestion that new clusters were produced within the minimum time need to acquire an NMR scan after hydride addition (202.2 ppm and 205.2 ppm, Fig. S47†). When the reaction was stopped after 30 minutes of stirring, only cluster **4** was observed, supporting HPLC/MS data that show loss of the Au_{14} species and the formation of **4** as the

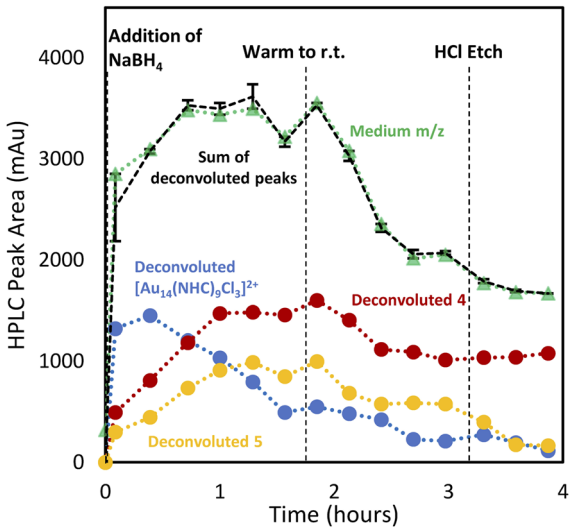

Fig. 5 Peak deconvolution of 8.5–9 min retention time window: red circle (**4**). Yellow circle (**5**), blue circle ($[Au_{14}(NHC)_9Cl_3]^{2+}$). Integrated sum for all deconvoluted signals is shown *via* black dashed line. Error bars indicate the difference between the sum of the deconvoluted peak fit and observed HPLC peak area (green line) for the same 8.5–9 min retention time window.

reaction progresses (ESI, Fig. S49†). These results are consistent with the Au_{14} cluster being a kinetic product that is quickly converted to more stable species.

Reaction monitoring during synthesis of $[Au_{24}(NHC)_{14}Cl_2H_3][BF_4]_3$

Having demonstrated the utility of LC/MS monitoring in the reduction of NHC–Au–Cl (**1**) to **4**, we then studied the reduction of [NHC–Au–Py]BF_4 (**2**) (Py = pyridine) to generate ($[Au_{24}(NHC)_{14}Cl_2H_3][BF_4]_3$) (**5**) (Fig. 1B).[30] Reaction monitoring was carried out as previously described, using **2** dissolved in toluene with 1.0 equivalent of $NaBH_4$ in EtOH. As observed in the reduction of **1**, the addition of a full equivalent of $NaBH_4$ led to the immediate consumption of **2**, and formation of NCs in the small *m*/*z* region along with **5** (Fig. 6).

In contrast to the synthesis of **4**, the reaction proceeded with the rapid formation of small clusters and then a slow increase in the medium *m*/*z* region NCs, while larger NCs were not formed significantly. Interestingly, the pyridine-ligated Au starting material, [NHC–Au–Py]BF_4 (**2**), was not regenerated during the reaction, with $[NHC–Au(I)–NHC]^+$ (**3**) being the only molecular species observed (Fig. 6). This is likely attributed to the presence of the non-coordinating BF_4^- anionic ligand in contrast to Cl^- which is present in higher concentration during the preparation of $[Au_{13}(NHC)_9Cl_3]Cl_2$ (**4**). After the rapid generation of compound **3**, 48% of this species goes on to be consumed over the course of the reaction (Fig. 6A–D). Thus, under low halide conditions, **3** appears to be involved in cluster formation, rather than acting only as a sink for free NHC as in the preparation of **4**. Interconversions between clusters are also clearly important for growth of medium sized clusters, based on the gradual decline of clusters in the small region.

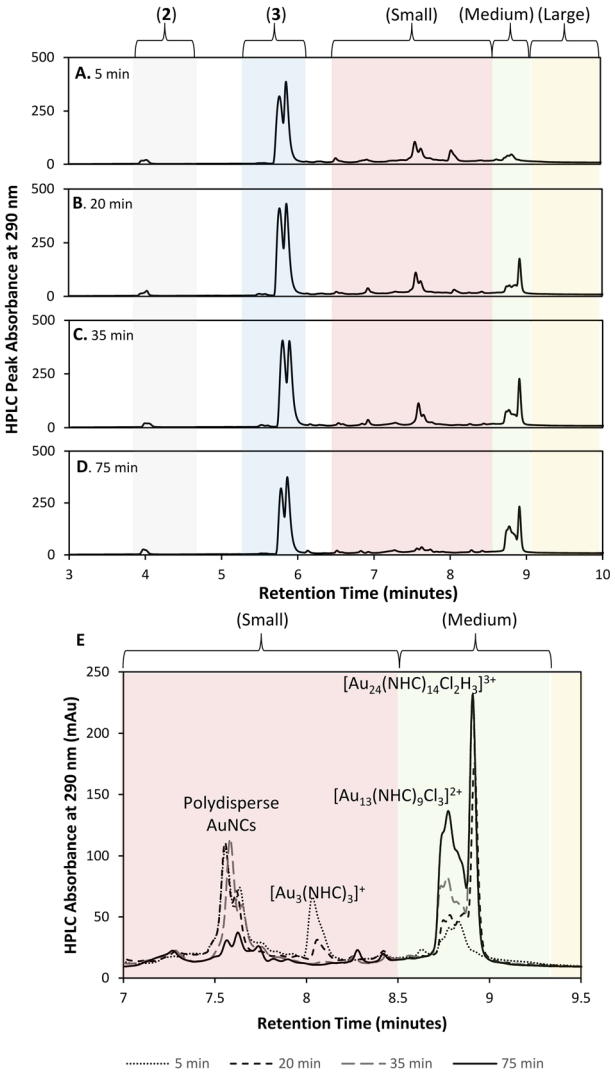

Fig. 6 Chromatograms of the synthesis of **5** taken at four critical points in the reaction with regional analysis size regions identified and highlighted. Sample 5 (A), 20 minutes (B), 35 minutes (C), and 75 minutes after the addition of $NaBH_4$ (D). (E) Small and medium region of the HPLC chromatogram highlighting major species and their evolution with time.

A detailed analysis of clusters in the small and medium *m*/*z* regions shows that after 15 min, the reaction mixture consists primarily of small clusters of unknown structure (rt = 7.5 min), **4** and $[Au_3(NHC)_3]^+$, an interesting cluster analogous to those synthesized by Sadighi and Bertrand (Fig. 6E).[33,34] As the reaction progresses, **5** appears, **4** increases in intensity and $[Au_3(NHC)_3]^+$ decreases. By 35 minutes into the reaction, the intensity of **5** is constant and $[Au_3(NHC)_3]^+$ has been consumed. After this point, the only changes observed in the cluster region are due to continued growth of **4** (likely along with related clusters) and the loss of smaller clusters eluting at about 7.5 minutes, which comprise several polydisperse species which could not be assigned definitive formulae due to the MSD signal complexity and low resolution of the MS. Although **3** continues to decrease during this time, and therefore likely remains engaged in cluster synthesis, these observations highlight the

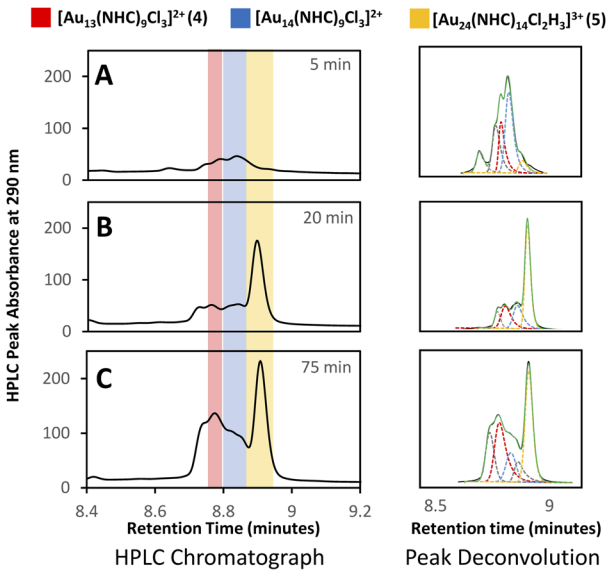

Fig. 7 Chromatograms of the medium region of the synthesis of **5** and deconvoluted peak shape taken at four critical points in the reaction with regional analysis size regions identified and highlighted. Sample 5 minutes (A), 20 minutes (B), 35 minutes (C), and 75 minutes after the addition of $NaBH_4$.

involvement of small clusters in the preparation of clusters **4** and **5**.

Deconvolution of the 8–9 min retention time window using our peak fitting algorithm provides a visual representation of the observations (Fig. 7). Interestingly, $[Au_3(NHC)_3]^+$ and **5** exhibited a strong correlation, evidenced by the decrease in $[Au_3(NHC)_3]^+$ concomitant with the cessation of the increase in

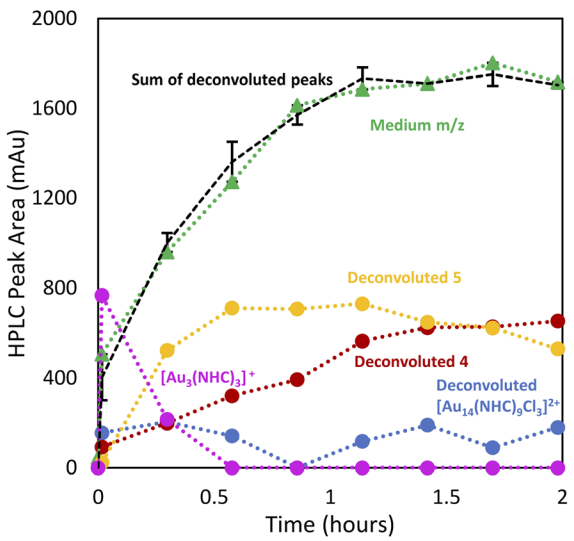

Fig. 8 Peak deconvolution of 8.5–9 min retention time window: red circle (**4**). Yellow circle (**5**), blue circle ($[Au_{14}(NHC)_9Cl_3]^{2+}$). Integrated sum for all deconvoluted signals is shown *via* black dashed line. Error bars indicate the difference between the sum of the deconvoluted peak fit and observed HPLC peak area (green line) for the same 8.5–9 min retention time window.

species **5** around the 35 minute mark (ESI, Fig. S3†). Comparison of high-halide conditions employed in the synthesis of **4** (Fig. 3), with the low halide conditions used for cluster **5** is instructive.

Both clusters are observed under the two conditions, while under low-halide conditions, cluster **5** is present from the early stages of the reaction and is accompanied by minor amounts of **4**. Under high halide conditions, cluster **5** grows in at longer reaction times, but is removed upon acid etch and purification.

Optimization of the synthesis of $[Au_{13}(NHC)_9Cl_3]Cl_2$ (4)

To optimize the synthesis of cluster **4**, we examined whether we could prevent the formation of large clusters by balancing the rate of reduction of precursor **1** with that of cluster evolution. This strategy aligns with prior work with thiol-protected AuNCs, which demonstrated that restricting the amount of $NaBH_4$ can improve selectivity and prevent the formation of undesired NCs.[20] Interestingly, $[(RS)_2Au]^-$ byproducts were also observed in this study.

Thus, we explored the use of stepwise dosing of $NaBH_4$. A solution of **1** in DCM was first prepared and sampled at 15 min time intervals by HPLC-MS over a 45 min period to ensure a stable initial baseline (Fig. 9A). The reducing agent ($NaBH_4$) was then added in 0.2 equivalents aliquots along with HPLC-MS analysis (Fig. 9B).

The first addition of $NaBH_4$ caused 40% of **1** to be consumed upon mixing, producing mainly bisNHC complex (**3**) and AuNCs in the small and medium *m*/*z* regions. The reaction was allowed to age for 15 min (Fig. 9C), resulting in increases in large clusters, while the small and medium clusters decreased. More surprisingly, a decrease in bisNHC complex (**3**) with a corresponding increase in **1** was also observed. Longer ageing times without additional $NaBH_4$ did not result in further changes to the chromatogram. Adding a second 0.2 equivalents of $NaBH_4$, followed by an additional 15 min pause in dosing gave similar observations: rapid consumption of **1**, resulting in an increase in **3** as well as formation of AuNCs in the small and medium *m*/*z* regions. A rebound in the concentration of **1** is also observed with concomitant reduction of **3** as small AuCNs evolve to medium and large species (Fig. 9D and E).

The observed rebound in the concentration of **1** suggests that a highly dynamic and reversible process is occurring during cluster formation, where unstable Au–NHC intermediates both aggregate to grow larger complexes but also degrade back to **1**. Although this experiment provides a limited view into the rapid, underlying process, it illustrates that the growth of these nanoclusters proceeds *via* the generations of transient, kinetically-favoured species, which give way to particular clusters that display far greater thermodynamic stability. This dynamic exchange favours growth to larger species, provided sufficient concentration of an activated cluster precursor (formed by reaction between $NaBH_4$ and **1**) is available. In the

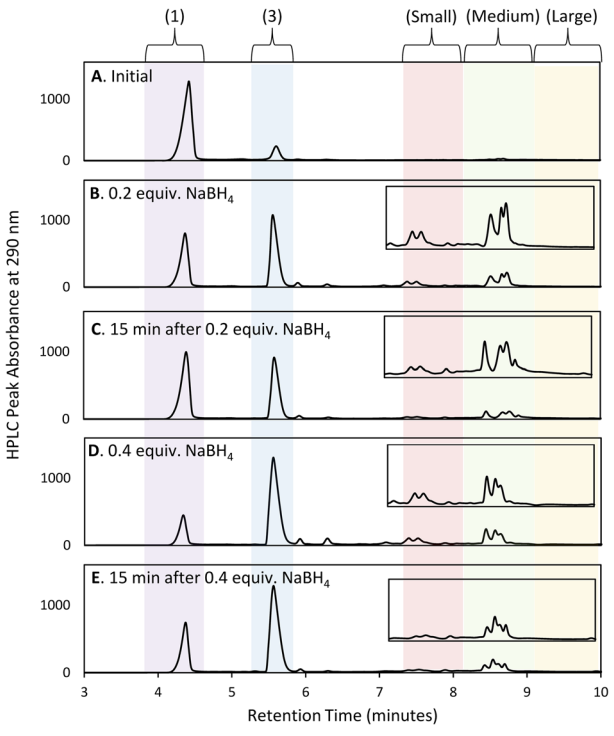

Fig. 9 Chromatograms for synthesis of **4** *via* dose-wise addition of $NaBH_4$ with regional analysis zones identified and highlighted. Sample taken before the addition of $NaBH_4$ (A), immediately following first addition of 0.2 equiv. $NaBH_4$ (B), and 15 min after $NaBH_4$ (C), additional 0.2 equiv. $NaBH_4$ (0.4 equiv. cumulative total) (D) and 15 min delay (E).

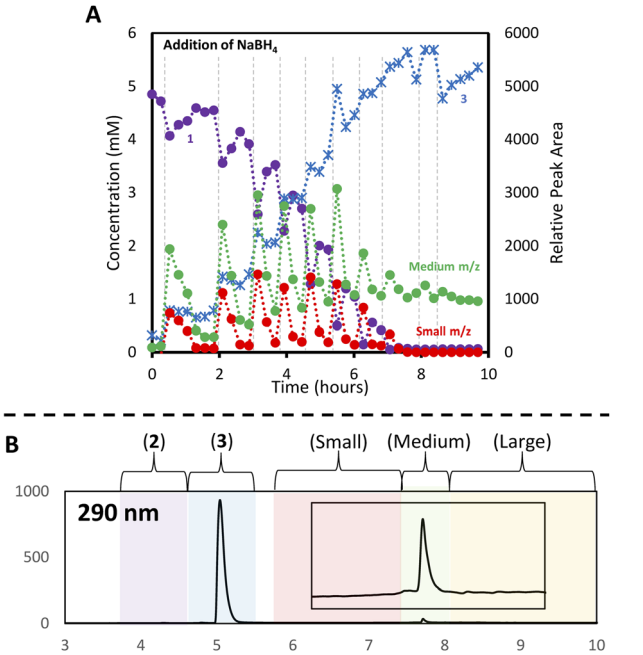

Fig. 10 HPLC time-course for dose-wise synthesis of AuNC **4**. (A) Change is components visualized *via* regional analysis. Left axis: starting material (**1**) and intermediate (**3**) quantified *via* internal standard; right axis: relative integral of respective size region normalized *vs.* internal standard; red circles (small region), green circles (medium region). Ten equal doses of 0.1 equiv. $NaBH_4$ in EtOH added at demarcated times; (B) chromatogram at endpoint reveals **4** is the only persistent AuNC under these conditions.

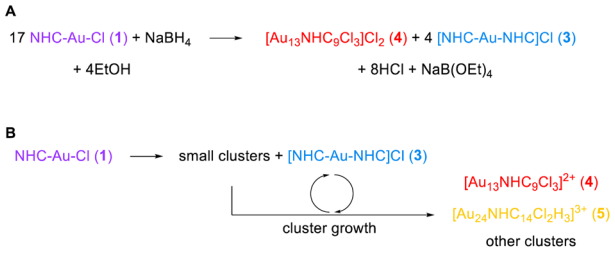

Scheme 1 (A) Balanced equation for the formation of NHC–AuNCs from reduction of **1** (B) potential pathways for the release of Au(I) precursors and route to AuNCs.

absence of sufficient reducing agent, unstable clusters may shed an Au–NHC unit, allowing regeneration of **1**.

The stepwise dosing method not only offers a detailed visualization of the AuNC's incremental growth but also yields higher concentrations of the desired Au_{13} (**4**), as evidenced by its relative peak area. This enhancement likely stems from effectively regulating the production rate of smaller AuNC precursors conducive to growth, and simultaneously reducing the transition of **4** into larger AuNC forms. To quantify the impact of this dosing strategy on gold nanocluster formation, we executed experiments with different $NaBH_4$ dosing schedules (0.2 equivalents added five times and 0.1 equivalents added ten times), benchmarking results using an internal standard (Fig. 10). The results reveal that each $NaBH_4$ aliquot causes a transformation: initial materials quickly change to intermediate **3** and various amounts of both small and medium AuNCs. Delaying subsequent $NaBH_4$ doses allows for starting material **1** to regenerate, accompanied by the consumption of both small and medium AuNCs. Once all Au–NCH **1** was consumed (around 7.5 hours, approximately 0.8 equiv. $NaBH_4$), further reducing agent inclusions have minimal impact on the reaction mixture. Notably, the slow-dosing trial yielded a 12% rise in the estimated yield of cluster **4**, as inferred from its quantitative peak area relative to the internal standard (see ESI, Fig. S38†). Moreover, at the reaction's conclusion, AuNC **4** emerged as the sole nanocluster present, even without applying an HCl etch.

Conclusions

Insights from these reaction monitoring studies have enabled us to generate a reasonable balanced reaction equation for the formation of cluster **4** (Scheme 1A). In this equation, the formation of compound (**3**) is explained by the necessary generation of Au atoms in the cluster that are not ligated by an NHC – the central Au atom, and the three atoms bound to chloride. Thus, the formation of one molar equivalent of cluster **4** from **1** requires the loss of four NHCs. These free NHCs react with **1**, resulting in the formation of four molar equivalents of **3** (Scheme 1A).

However, this equation neglects the complex mechanism by which even simple clusters like **4** are prepared. Our studies have shown that small clusters such as $Au_3(NHC)_3^+$ are key precursors. As these evolve, and as clusters become larger, more unligated gold atoms are produced, leading to the generation of **3** or possibly even regenerating starting materials **1** (Scheme 1B). Depending on the reaction conditions, specifically the amount of halide present, **3** can also be involved in the preparation of larger clusters (Scheme 1B).

Interconversion within a size range, for example from $[Au_{14}(NHC)_9Cl_3]^{2+}$ to **4**, also needs to be considered as it has been documented in this study (Fig. 3, 5, and 8). The time at which the reaction is deemed complete and the use or not of post-synthesis treatments, for example with HCl, will result in completely different cluster compositions, as illustrated in Fig. 5. More importantly, the rate of addition of reducing agent can be tuned to mitigate the generation of cluster forming precursors, thus improving the mass throughput to desired nanoclusters. This focusing behavior coupled to control of the rate of reduction provides a novel means of control when coupled to the HPLC time-course visualization.

The nature of the reaction of $NaBH_4$ with the starting gold complex **1** has not been addressed in this study, but likely proceeds through the initial generation of gold hydrides, species that can be isolated in the case of very bulky NHCs.[35] The observation of clusters that retain the hydride ligand supports this possibility.[30]

Overall, this study demonstrates the importance of real-time reaction monitoring using HPLC-MS and ^{13}C-NMR spectroscopy to provide insights into true reaction compositions during the preparation of NHC-protected gold nanoclusters. In depth analysis revealed the formation of previously unidentified intermediates including an Au_{14} cluster of moderate stability and an $Au_3(NHC)_3^+$ cluster related to the first ever prepared Au–NHC clusters. Our analysis also revealed the critical importance of transformations between clusters of different sizes and outlines potential routes for optimization such as sequential *vs.* single additions of reducing agents. Insights into the mechanism of nanocluster formation have also included a balanced reaction equation to understand and predict the by-products of cluster-forming reactions.

Data availability

All code needed to execute the HPLC deconvolution is freely available *via* online repository at **https://gitlab.com/heingroup/hplc_peak_deconvolution**.

Author contributions

J. L. and Y. S. performed the development of HPLC methods, and analysed reaction monitoring data under the supervision of J. E. H. V. K. K. and A. I. S. performed NMR studies, and synthesis of control materials under the supervision of C. M. C. W. Z. created and implemented the code to deconvolute the HPLC traces. C. M. C. and J. E. H. jointly conceived of the project. All authors wrote the manuscript, ESI† methods, and related materials.

Conflicts of interest

There are no conflicts to declare.

Acknowledgements

V. K. K. and A. I. S. acknowledge the Ontario Government and NSERC for support. Emiliya Rafikova is acknowledged for her contribution to the project. Financial support for this work was provided by The University of British Columbia, Queen's University, the Canada Foundation for Innovation (CFI; CFI-35883 and CFI-33355) the Natural Sciences and Engineering Research Council of Canada (NSERC; RGPIN-2021-03168, RGPIN/04667-2016, Discovery Accelerator Supplement), and the New Frontiers in Research Fund – Exploration program (NFRFE-2019-01334, NFRFT-2020-00573).

Notes and references

§ When H_2O/MeCN with 0.1% formic acid (FA) was employed as a mobile phase in place of MeOH a significant new peak was observed at a different retention time than **3** (Fig. 1D). This peak was identified as $[NHC–Au(I)–MeCN]^+$ based on the observed mass signal (*m*/*z* 536.0) (ESI, Fig. S35†). This suggests that MeCN behaves as a nucleophilic solvent and exchanges with the Cl^- ligand. The insolubility of **4** in MeCN was also problematic and prompted the use of MeOH as an alternative.

¶ Dissolution of starting material **1** in the reaction solvent gave the expected signal for **1**, along with a small amount of **3**, even prior to the addition of $NaBH_4$, indicating that species **3** is readily produces in chlorinated solvents.

‖ No mass signals were observed in the large *m*/*z* region due to the *m*/*z* limit of the mass spectrometer (max *m*/*z* 3000) (see ESI S4†).

1 R. Jin, *Nanoscale*, 2015, **7**, 1549–1565.
2 H. Qian, M. Zhu, Z. Wu and R. Jin, *Acc. Chem. Res.*, 2012, **45**, 1470–1479.
3 Y. Du, H. Sheng, D. Astruc and M. Zhu, *Chem. Rev.*, 2020, **120**, 526–622.
4 R. Jin, C. Zeng, M. Zhou and Y. Chen, *Chem. Rev.*, 2016, **116**, 10346–10413.
5 M. Zhou, X. Du, H. Wang and R. Jin, *ACS Nano*, 2021, **15**, 13980–13992.
6 M. R. Narouz, K. M. Osten, P. J. Unsworth, R. W. Y. Man, K. Salorinne, S. Takano, R. Tomihara, S. Kaappa, S. Malola, C. T. Dinh, J. D. Padmos, K. Ayoo, P. J. Garrett, M. Nambo, J. H. Horton, E. H. Sargent, H. Häkkinen, T. Tsukuda and C. M. Crudden, *Nat. Chem.*, 2019, **11**, 419–425.
7 M. R. Narouz, S. Takano, P. A. Lummis, T. I. Levchenko, A. Nazemi, S. Kaappa, S. Malola, G. Yousefalizadeh, L. A. Calhoun, K. G. Stamplecoskie, H. Häkkinen, T. Tsukuda and C. M. Crudden, *J. Am. Chem. Soc.*, 2019, **141**, 14997–15002.
8 H. Shen, S. Xiang, Z. Xu, C. Liu, X. Li, C. Sun, S. Lin, B. K. Teo and N. Zheng, *Nano Res.*, 2020, **13**, 1908–1911.
9 Z. Lei, M. Endo, H. Ube, T. Shiraogawa, P. Zhao, K. Nagata, X.-L. Pei, T. Eguchi, T. Kamachi, M. Ehara, T. Ozawa and M. Shionoya, *Nat. Commun.*, 2022, **13**, 4288.
10 H. Yi, K. M. Osten, T. I. Levchenko, A. J. Veinot, Y. Aramaki, T. Ooi, M. Nambo and C. M. Crudden, *Chem. Sci.*, 2021, **12**, 10436–10440.
11 H. Ramsay, D. Simon, E. Steele, A. Hebert, R. D. Oleschuk and K. G. Stamplecoskie, *RSC Adv.*, 2018, **8**, 42080–42086.
12 X.-K. Wan, Z.-J. Guan and Q.-M. Wang, *Angew. Chem., Int. Ed.*, 2017, **56**, 11494–11497.
13 X. Han, X. Luan, H. Su, J. Li, S. Yuan, Z. Lei, Y. Pei and Q. Wang, *Angew. Chem.*, 2020, **132**, 2329–2332.
14 L. Liao, J. Chen, C. Wang, S. Zhuang, N. Yan, C. Yao, N. Xia, L. Li, X. Bao and Z. Wu, *Chem. Commun.*, 2016, **52**, 12036–12039.
15 M. Agrachev, M. Ruzzi, A. Venzo and F. Maran, *Acc. Chem. Res.*, 2019, **52**, 44–52.
16 A. W. Cook and T. W. Hayton, *Acc. Chem. Res.*, 2018, **51**, 2456–2464.
17 Y. Negishi, K. Nobusada and T. Tsukuda, *J. Am. Chem. Soc.*, 2005, **127**, 5261–5270.
18 G. Yousefalizadeh and K. G. Stamplecoskie, *J. Photochem. Photobiol., A*, 2018, **353**, 251–254.
19 Z. Luo, V. Nachammai, B. Zhang, N. Yan, D. T. Leong, D. Jiang and J. Xie, *J. Am. Chem. Soc.*, 2014, **136**, 10577–10580.
20 T. Chen, V. Fung, Q. Yao, Z. Luo, D. E. Jiang and J. Xie, *J. Am. Chem. Soc.*, 2018, **140**, 11370–11377.
21 Y. Shichibu and K. Konishi, *Small*, 2010, **6**, 1216–1220.
22 Y. Negishi, S. Hashimoto, A. Ebina, K. Hamada, S. Hossain and T. Kawawaki, *Nanoscale*, 2020, **12**, 8017–8039.
23 Y. Niihori, C. Uchida, W. Kurashige and Y. Negishi, *Phys. Chem. Chem. Phys.*, 2016, **18**, 4251–4265.
24 Y. Zhang, Q. Hu, M. C. Paau, S. Xie, P. Gao, W. Chan and M. M. F. Choi, *J. Phys. Chem. C*, 2013, **117**, 18697–18708.
25 S. Xie, M. C. Paau, Y. Zhang, S. Shuang, W. Chan and M. M. F. Choi, *Nanoscale*, 2012, **4**, 5325–5332.
26 S. Bordawekar, A. Chanda, A. M. Daly, A. W. Garrett, J. P. Higgins, M. A. LaPack, T. D. Maloney, J. Morgado, S. Mukherjee, J. D. Orr, G. L. Reid, B. S. Yang and H. W. Ward, *Org. Process Res. Dev.*, 2015, **19**, 1174–1185.
27 Y. Sato, J. Liu, A. J. Kukor, J. C. Culhane, J. L. Tucker, D. J. Kucera, B. M. Cochran and J. E. Hein, *J. Org. Chem.*, 2021, **86**, 14069–14078.
28 J. Liu, Y. Sato, F. Yang, A. J. Kukor and J. E. Hein, *Chem.: Methods*, 2022, **2**, e202200009.
29 M. R. Narouz, S. Takano, P. A. Lummis, T. I. Levchenko, A. Nazemi, S. Kaappa, S. Malola, G. Yousefalizadeh, L. A. Calhoun, K. G. Stamplecoskie, H. Häkkinen, T. Tsukuda and C. M. Crudden, *J. Am. Chem. Soc.*, 2019, **141**, 14997–15002.
30 V. K. Kulkarni, B. N. Khiarak, S. Takano, S. Malola, E. L. Albright, T. I. Levchenko, M. D. Aloisio, C. Dinh, T. Tsukuda, H. Häkkinen and C. M. Crudden, *J. Am. Chem. Soc.*, 2022, **144**, 9000–9006.
31 R. Jothibasu, H. V. Huynh and L. L. Koh, *J. Organomet. Chem.*, 2008, **693**, 374–380.
32 S. Misra, M. F. Wahab, D. C. Patel and D. W. Armstrong, *J. Sep. Sci.*, 2019, **42**, 1644–1657.
33 L. Jin, D. S. Weinberger, M. Melaimi, C. E. Moore, A. L. Rheingold and G. Bertrand, *Angew. Chem., Int. Ed.*, 2014, **53**, 9059–9063.
34 T. J. Robilotto, J. Bacsa, T. G. Gray and J. P. Sadighi, *Angew. Chem., Int. Ed.*, 2012, **51**, 12077–12080.
35 N. Phillips, T. Dodson, R. Tirfoin, J. I. Bates and S. Aldridge, *Chem.–Eur. J.*, 2014, **20**, 16721–16731.